Supporting Information for "Supersonic Impact Response of Polymer Thin Films via Large-Scale Atomistic Simulations"

Andrew L. Bowman[a], Edwin P. Chan[b], William B. Lawrimore[a], John K. Newman[a]*

[a] Engineer Research and Development Center, 3909 Halls Ferry Rd., Vicksburg, MS 39180, United States of America
[b] Materials Science and Engineering Division, National Institute of Standards and Technology, 100 Bureau Drive, Gaithersburg, MD 20899, United States of America
*: Corresponding author (Phone: 662-769-7231), Email: andrew.l.bowman@usace.army.mil

Simulation Methodology

Pre-processing and simulation of ballistic impacts on polymer thin films of polyethylene (PE) and polystyrene (PS) are conducted through a multistep process involving initial film construction, equilibration at melt temperature (600 K), annealment to room temperature (300 K), additional equilibration at room temperature, and finally impacts at various incident velocities. A stepwise overview of the simulation process is illustrated in Figure S1 for a PE thin film. The process is the same regardless of polymer type.

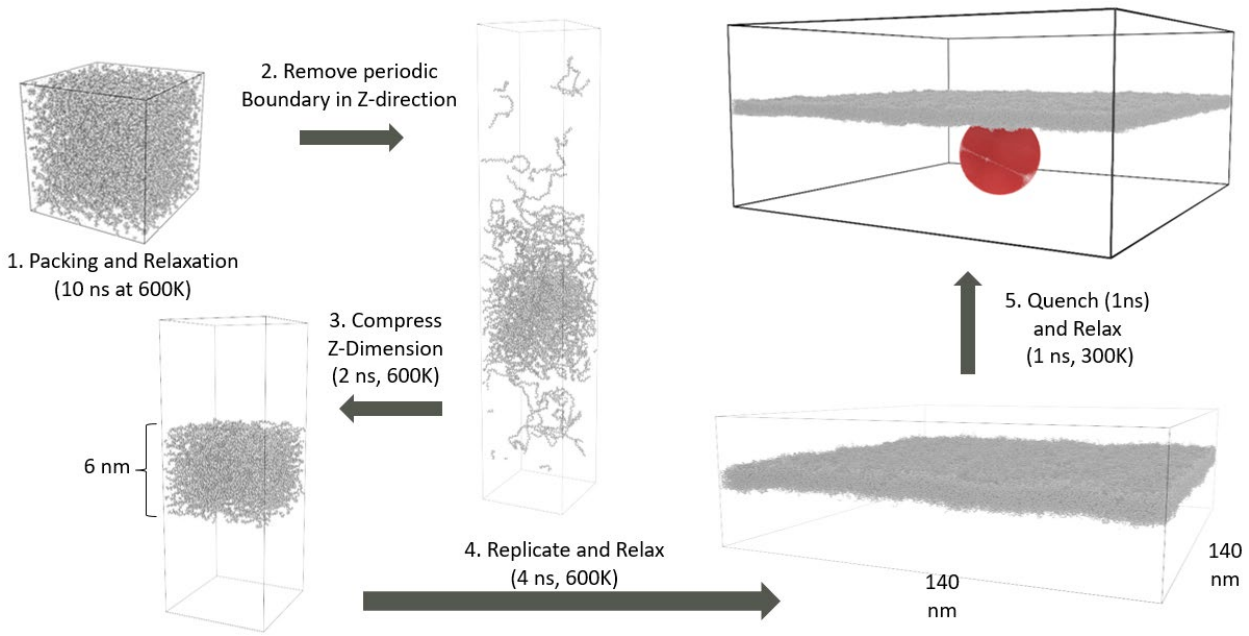

Figure S1. Stepwise overview of the simulation process of initial construction, relaxation, equilibration, and impact.

Initially, amorphous 3D periodic structures are packed using the web-based nanoHUB Polymer Modeler[1] tool with ten chains, each consisting of 1,000 carbon atoms, corresponding to molecular weights (M_n) of 14 kg/mol and 52.1 kg/mol for PE and PS, respectively. Terminal carbon atoms for each chain were terminated with hydrogen to achieve saturated structures. The amorphous structure files are exported to the Large-scale Atomic/Molecular Massively Parallel Simulator

(LAMMPS)[2] for minimization and equilibration with the DREIDING[3] potential. The structures are equilibrated using a time step of 2 fs with a constant number of atoms, pressure, and temperature (NPT) dynamics at zero pressure for 10 ns at a melt state of 600 K. This process of equilibration was shown to fully relax the entanglements of PE systems[4]. For all thermostats and barostats, dampening parameters of 100 and 1,000 time steps were used to dampen the temperature and pressure respectively. Equilibration at melt temperature ensures the full relaxation of kinks and entanglements and creates a well equilibrated initial structure. After initial equilibration, periodicity of the z-direction is removed, maintaining 2D periodicity in the x and y dimensions; and two fix wall commands in LAMMPS are used to push the polymer chains from the +z and –z directions to the desired film thickness while allowing the lateral faces (x and y) to relax. The wall is subsequently held at 600 K with NPT conditions in the x and y directions for 1 ns then removed for 1 ns. This creates the stable thin film structure seen in Figure S1 at the end of Step 3. Next, the stable thin films are replicated in the x and y dimensions to create the desired slab size (140 nm x 140 nm). Again, to relax the repeating segments, the large thin films are equilibrated at 600 K with NPT boundaries in the x and y directions for an additional 4 ns. Then the films are quenched from 600 K to 300 K with a constant number of atoms, volume, and temperature (NVT) dynamics over a time of 1 ns, then held at 300 K for an additional 1 ns. Finally, the thin films are equilibrated for 0.5 ns at 300 K using either the AIREBO[5] or MEAM[6], potential producing well-equilibrated thin film structures ready for impact simulations. The time step of 0.4 fs was used for equilibration with AIREBO and MEAM as reactive potentials do not have explicitly defined bonds and hydrogen atoms can be easily lost with elevated time steps.

After equilibration at 300 K, thin films were subjected to impact by a spherical projectile with a range of initial supersonic and hypersonic velocities (0.5 – 5 km/s). A time step of 0.3 fs was used

to capture the atom displacement during impact. For the projectile, with a diameter of 30 nm, a diamond lattice structure was used with a lattice constant of 7.14 Å and a bead mass of 96.1 g/mol. Interactions between the projectile and the thin film are modeled by a typical 12-6 Lennard-Jones potential with ε_{lj} = 0.0085 eV and σ_{lj} = 3.46 Å. The projectile is treated as a rigid body throughout impact. These values have been investigated and found to have negligible effect on the impact response, as the impactor is observed to stay rigid and friction between the impactor and thin films is small during impact[7]. Areas around the edges of the thin film spanning 40 Å are fixed (via setforce command) to mimic the clamping of the films similar to LIPIT experiments. Following recommendations of previous ballistic impact MD simulations[7], a ratio of projectile radius (R) to film thickness (t) of 2.5 was implemented, along with a thin film side length of eight projectile radii. The projectile was placed close to the bottom surface of the films, and an upward initial velocity was given to the projectile. An NVE (constant number of atoms, volume and energy) ensemble is used to integrate the system dynamics during the impact event.

Post-Processing

Kinetic Energy, Temperature, and Pressure Calculation

The kinetic energy of the projectile is output every 10 time steps and is used to calculate the energy absorbed by the thin films (E_p^*). E_p^* is defined as the loss of Kinetic Energy (KE) of the projectile normalized by the mass of the thin film contained within the projectile's projected impact area and is used as a metric to compare dissimilar materials. To calculate the film temperature evolution, a temperature compute that removes the center-of-mass velocity (compute temp/com) was used in LAMMPS to calculate the temperature of a group of atoms bound by the projected area of the projectile. As the temperature around the impact site is inhomogeneous, there is a spatial distribution of temperatures with higher temperatures located closer to the initial impact

site. Figure S2 illustrates the distribution of temperature emanating from the initial contact point (black circle in Figure s2). The average temperature of the area bounded by the projectile diameter was used in the manuscript. Similarly, a pressure compute of a group of atoms bounded by the projected area of the projectile is defined. This computes a pressure*volume, therefore the compute was divided by the volume of the thin film within the projected area (area*film thickness) to produce pressure.

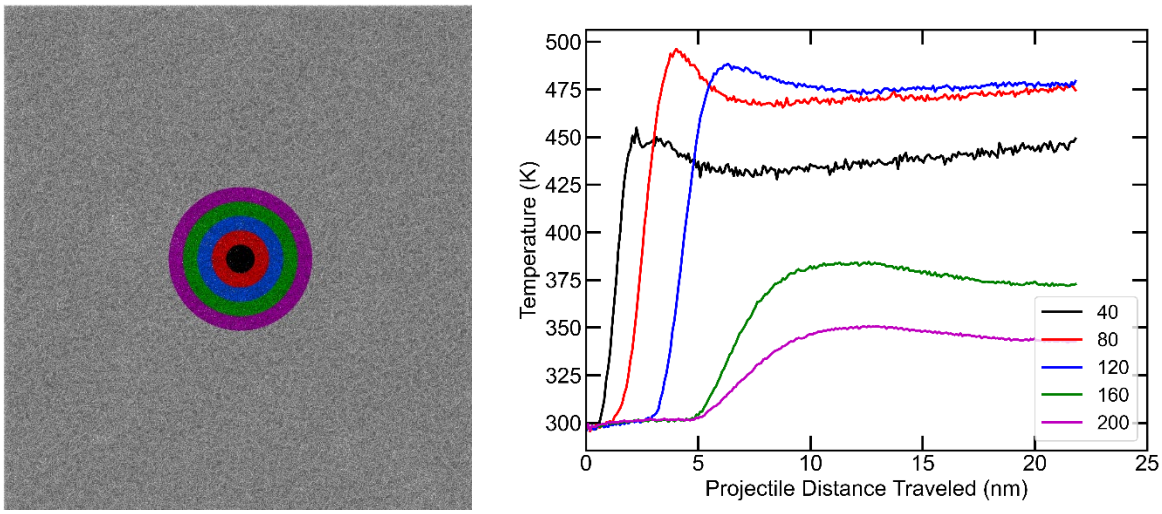

Figure S2: Example of the spatial temperature distribution during a 1.5 km s^{-1} impact on PE cooresponding to circlular areas with a radius of 40-200 Å.

Film Characterization

Careful characterization of the simulated thin films is important in order to properly establish structure-property relationships. Figure S3 illustrates the density distributions of the thin films along with the Voronoi volume profiles (atomic volume). The density distribution was calculated by binning the thin film (100 bins) along the z-dimension (thickness) and determining the density of each bin by totaling the atomic weight of the atoms within each bin divided by the bin volume. The atomic volumes were calculated using the Voronoi Analysis feature of the Open Visualization

Tool (OVITO)[8] to calculate the local volume of each atom and then plotted against the z-coordinate of the respective atom.

Using the density distribution in Figure S3, the average film density can be calculated by averaging the density of each bin weighted by the number of atoms in each bin. Similarly, the average film thickness can be determined by averaging the z-position of each bin weighted by the number of atoms in each bin. This procedure produces estimated average film densities of 643 kg m^{-3} and 789 kg m^{-3} and film thicknesses of 4.8 nm and 4.9 nm for PE and PS, respectively. Note, by taking into account the near-surface lower density regions, the average film density is less than the bulk densities that appear at the center of the films (approximately 750 kg m^{-3} and 945 kg m^{-3}), and the average film thickness is slightly less than the target thickness of 6 nm. The PE considered in this work is in the completely amorphous state, as crystallization times are too long for MD simulations, which produces a density lower than experimentally observed semicrystalline PE. From analysis of the Voronoi volume profiles, the films contain centralized well-packed dense regions approximately 3-4 nm thick and then enter a transition region in which the local atomic volume increases (density decreases) as the surface is approached. Free surfaces have a strong influence on chain dynamics[9] by increasing chain mobility and lowering the entanglement density. The effect of free surfaces are emphasized by the observed transition regions (decreasing density regions) in Figure S3 and is broader in PS.

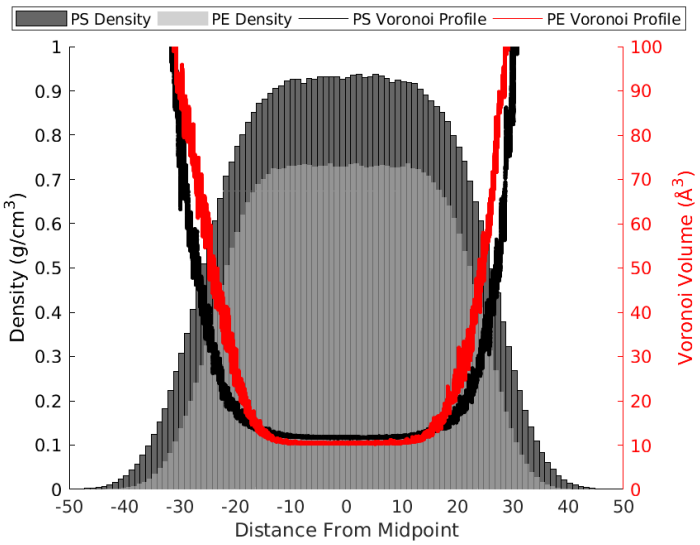

Figure S3. Density and atomic Voronoi volume profiles of amorphous PS and PE thin films indicating bulk high-density regions at the film center and low- density transition regions near the surface.

Bond Scission and Entanglement Density Calculation

Again, proper characterization is a key step in analysis of mechanical properties of materials. For postprocessing the evolution of broken bonds, OVITO[8] is used to visualize the perforation at various points during impact. The create bonds OVITO modifier is used to calculate the number of bonds for each snapshot in time (based on neighbor cut of distance) and to determine the loss of bonds over the course of impact for each bond type. For this work, bonds between each different types of atoms can rupture. Here, C-H, C-C, and C-phenyl (Ph) bonds were observed to rupture during impact. The total number of ruptured bonds versus impact velocity is illustrated in Figure S4. For an estimate of the total energy dissipated through bond breaking, bond energies of 3.58 ev/bond were assumed for C-C and C-Ph bonds and 4.28 ev/bond were assumed for C-H bonds. By multiplying the bond energy by the number of broken bonds and normalizing by the total amount of energy dissipation, the contribution of bond scission to energy dissipation can be

estimated as seen in Figure S4. Overall, the direct contribution of bond scission to energy dissipation is very low.

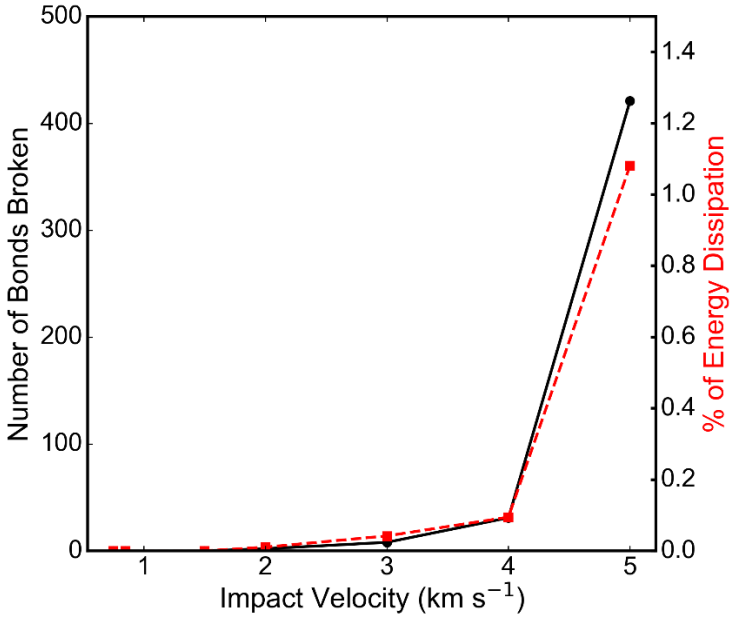

Figure S4. Number of broken bonds in PS versus impact velocity. The red line depicts the % of energy dissipation contributed through bond scission.

The entanglement density is quantified to study the influence of the entanglement density on energy absorption, as the two are thought to be highly related. The number of entanglements is not possible to count directly experimentally; therefore the ρ_e is typically estimated. In this work we estimate the ρ_e from the molecular weight (M_n) and entanglement length (M_e) in the same fashion as other experimental works[10,11] based on the entanglement network model of Bersted[12]:

$$\rho_e = \frac{2N_0\rho}{3M_c}\left(1 - \frac{M_c}{M_n}\right) \quad (1)$$

where N_0 is Avogadro's number, ρ is the film density, and $M_c \sim 2M_e$.

To maintain consistency between experiments and simulations, the simulated entanglement molecular weight must be determined (density and M_n have been previously defined). The complete connectivity network along the polymer backbone is easily defined by iterating through

the atoms sequentially, making the physical determination of entanglements possible. Several methods exist, such as the Z1[13–15] and CReTA[16] methods, for topologically determining the actual number of entanglements within the system. Use of reactive potentials can cause difficulties in determining the connectivity network during deformation when bond scission and bond reformation are likely, but determining the connectivity is typically trivial at the end of the equilibration step before stress is applied to the system. The Z1 algorithm can give the number of entanglements per chain along with additional data, such as the entanglement length. The ρ and M_n for the model PS and PE were given earlier, and the M_e (2.3 and 25.8 kg mol^{-1} for PE and PS) is found using the Z1 algorithm to determine the entanglement length of the given system.

Comparison of AIREBO and MEAM Potentials

In order to investigate the influence of bond breaking vs. disentanglement, a reactive (bond breaking/forming) atomistic potential is required. Three well suited options exist: AIREBO[5], MEAM[6], and Reactive Force Field (ReaxFF)[17]. ReaxFF is highly accurate; however, it incurs the highest computational burden and is about an order of magnitude slower than AIREBO or MEAM. Due to the size of the system and the already staggering computational undertaking, ReaxFF was not considered for further testing. MEAM has been used successfully to study high-rate deformation in PE[4] and is arguably more accurate than AIREBO. The pitfall for MEAM is that currently only saturated polymers are possible to simulate, which eliminates the MEAM for modeling PS. AIREBO is a computationally efficient reactive potential that has been successfully used to model both PE[18] and PS[19].

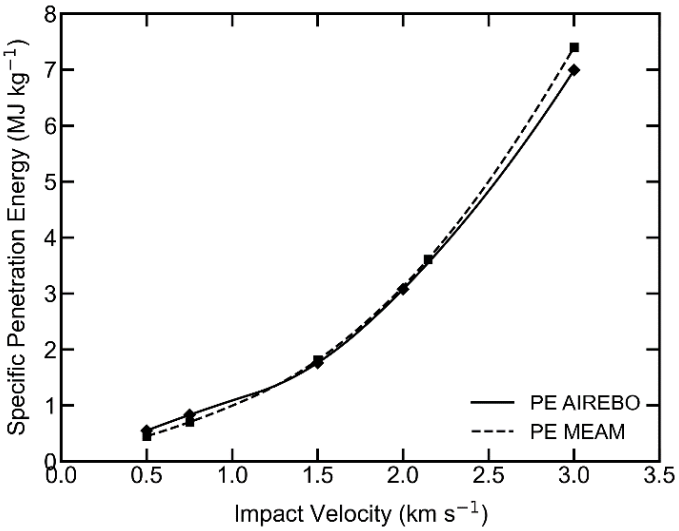

Figure S5. Comparison of the specific penetration energy prediction for AIREBO and MEAM potentials.

Impact simulations were conducted comparing the AIREBO and MEAM potentials specifically for use in studying high-rate impacts in PE thin films. Figure S5 illustrates the specific penetration energy (E_p^*) vs. impact velocity (V_i) response. Both potentials produce almost identical E_p^* vs. V_i curves and are computationally similarly efficient. However, discrepancies arise when the fracture behaviors at high velocities are compared. Figure S6 compares the impact responses of PE for the AIREBO and MEAM potential at various impact velocities. At low velocities (<1.5 km s^{-1}), the penetration behaviors are very similar. However, at higher velocities (> 3 km s^{-1}) significant degradation is observed in PE using the MEAM potential due to adiabatic heating, resulting in elevated film temperatures (~3000K) and severe bond disassociation of C-C (chain scission) and C-H (dehydrogenation) bonds. This thermal degradation is not captured with AIREBO, possibly due to a high C-C dissociation energy[6]. MEAM has also been shown to underpredict the heat of reaction involving C-C and C-H bonds compared to AIREBO[20], which most likely causes MEAM

172 to predict lower thermal degradation temperature. Therefore, it appears that AIREBO may slightly
173 underpredict degradation while MEAM slightly overpredicts degradation.

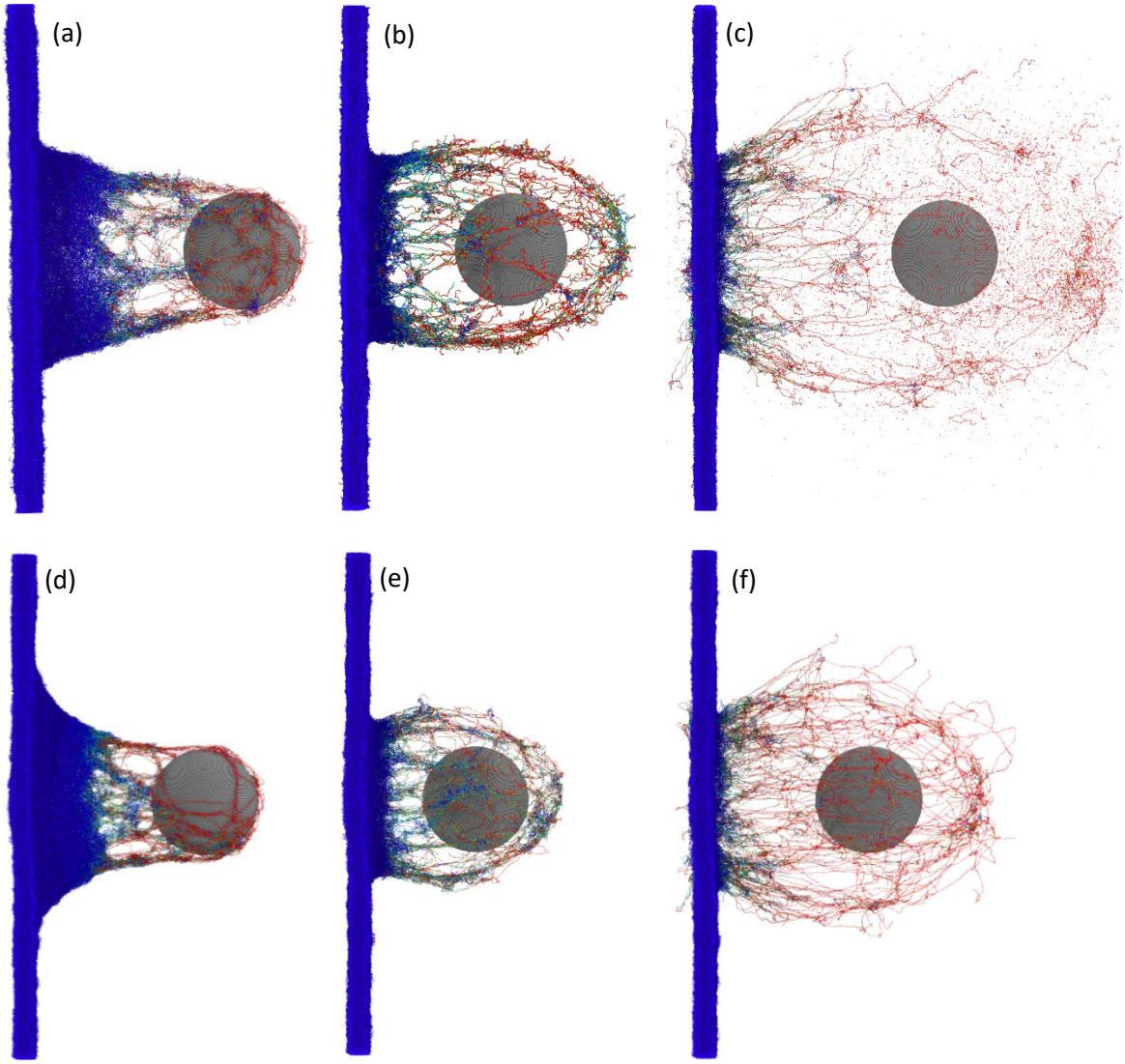

174
175

176 **Figure S6.** Snapshots of the ballistic failure modes for amorphous polyethylene using the (a-c)
177 MEAM potential and (d-f) AIREBO potential impacted at (a,d) 0.75 km s^{-1}, (b,e) 1.5 km s^{-1}, and
178 (c,f) 3 km s^{-1} illustrating similar ballistic penetration responses for both potentials at low velocity
179 while only the MEAM captures temperature degradation at elevated velocity (c).

180 Degradation is a complex property to capture using MD, and simulations have been shown to be
181 highly influenced by the rate of temperature change[21], leading to overprediction of degradation

temperatures. Illustrated in Figure S7, temperatures predicted by AIREBO span several thousand degrees. Hence, most of the analysis herein focuses on the supersonic impact regime before temperature degradation occurs. Additionally, for the ultrathin films studied, capturing the degradation at hypersonic velocities is not critical, as the projectile quickly passes through the film and energy is quickly dissipated (i.e., the projectile velocities decreases) before thermal degradation occurs (as observed with MEAM), hence not influencing the resulting E_p^* (Figure S5). Thus, even at higher impact velocities the specific penetration energies are nearly the same for AIREBO and MEAM. For much thicker films this could become an issue, as the projectile may not penetrate completely and degraded chains will be more impactful, and will need further investigation. One last point to consider is that the degradation point could be shifted due to the increase in degradation temperature seen in both PE and PS under high pressure[22]. Hence, polymers can still absorb tremendous amounts of energy during hypervelocity impacts, even though degradation occurs; and hydrocarbon based polymers, such as ultra-high molecular weight PE, have been suggested for use as shielding in aerospace applications[23].

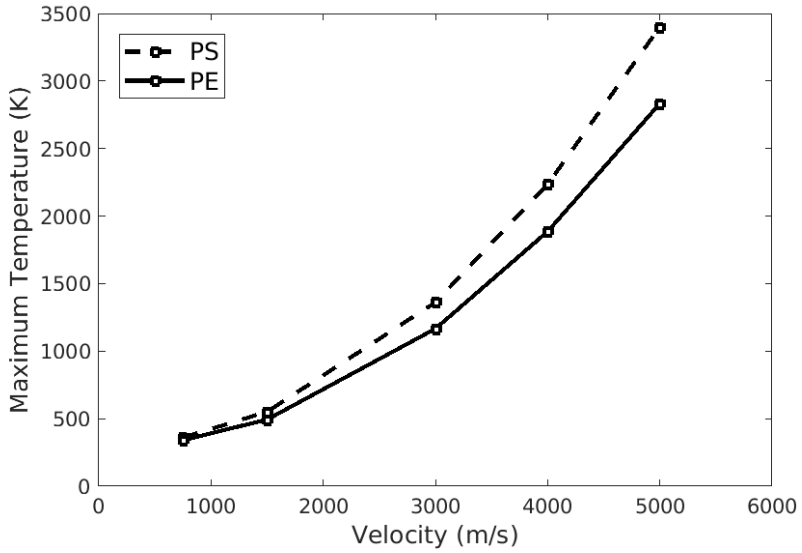

199

200 **Figure S7:** Maximum temperatures achieved during impact versus impact velocity for the

201 AIREBO potential.

Additional Visualizations of Projectile Penetration

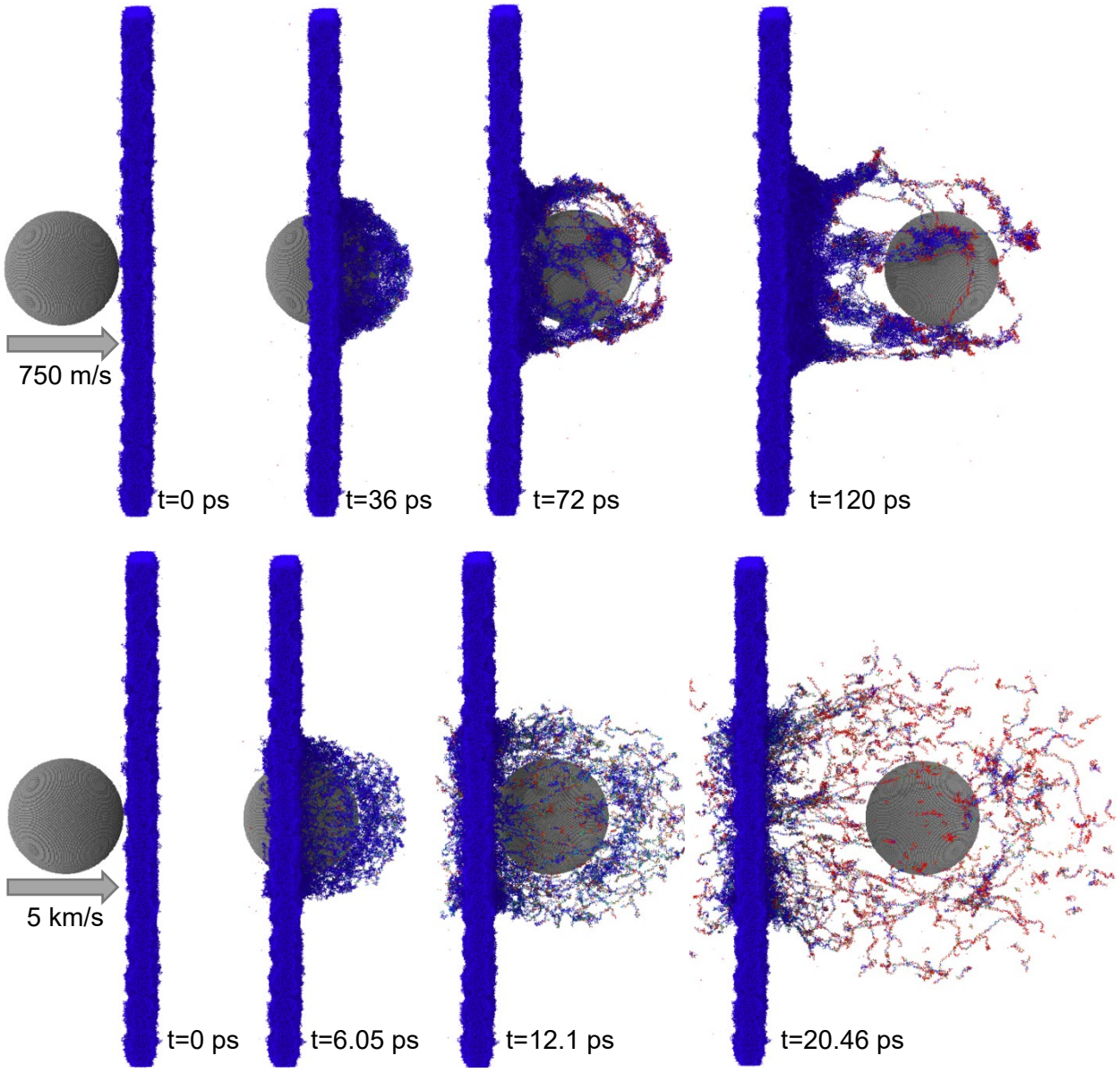

Figure S8. Snapshots of the progression of a ballistic impact event for PS at an impact of 750 m/s and 5 km/s at various time steps during penetration.

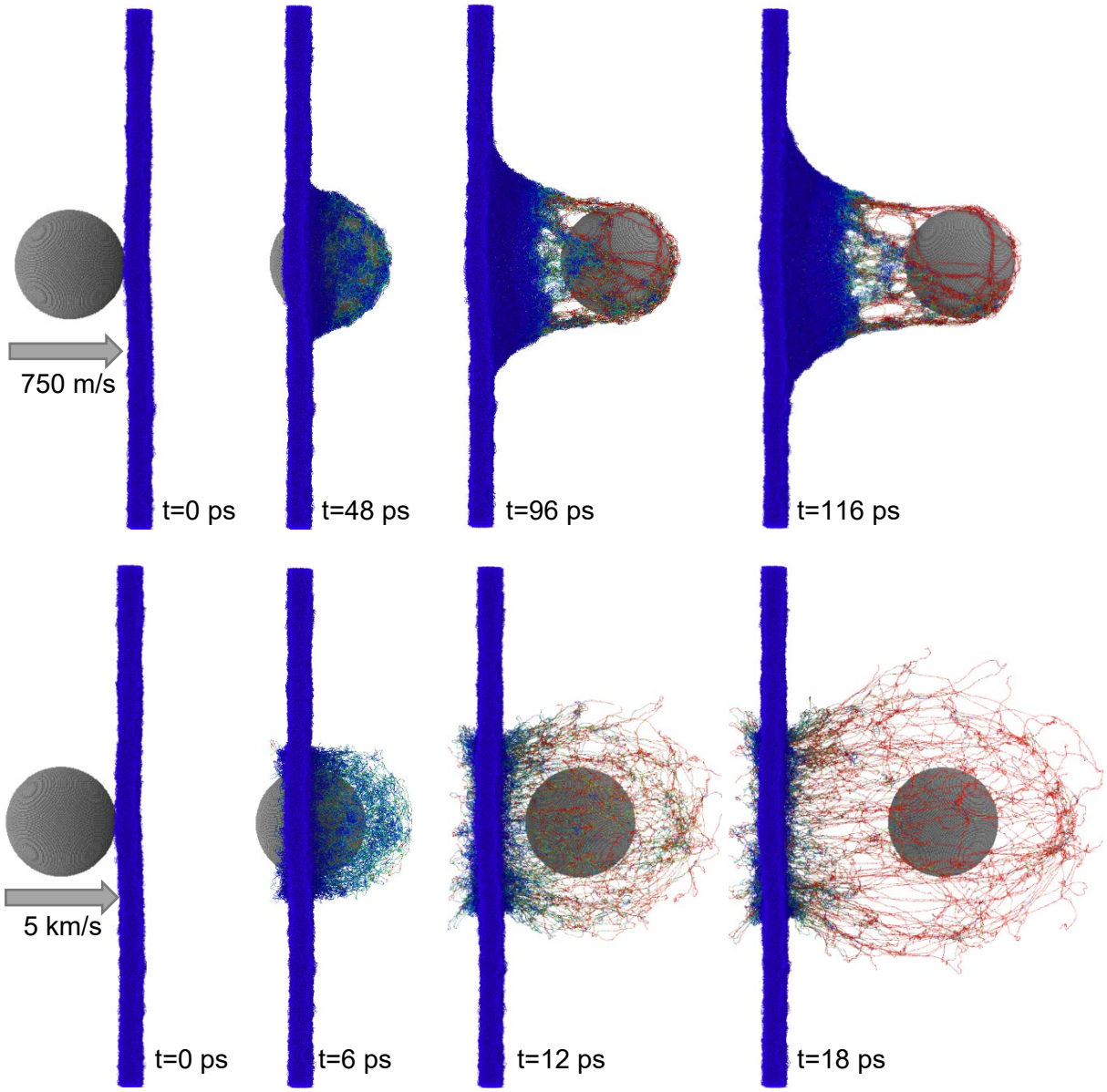

Figure S9. Snapshots of the progression of a ballistic impact event for PE at an impact of 750 m/s and 5 km/s at various time steps during penetration.

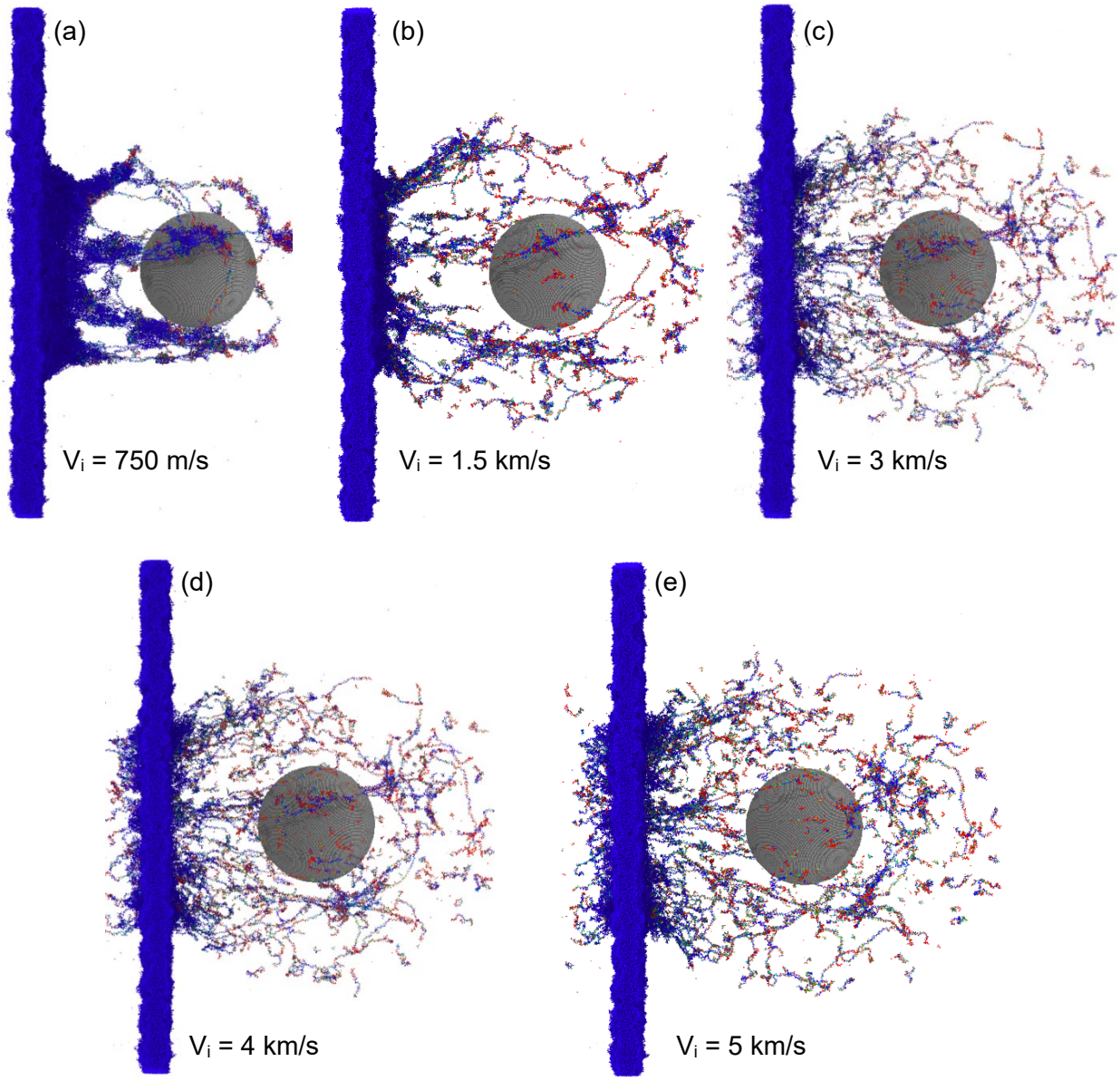

Figure S10. Snapshots of final ballistic penetration of PS for impact velocities of (a) 750 m/s, (b) 1.5 km/s, (c) 3km/s, (d) 4 km/s, and (e) 5 km/s. Failure transition from chain decohesion and petalling at low impact velocities to fragmentation and chain scission at high impact velocities.

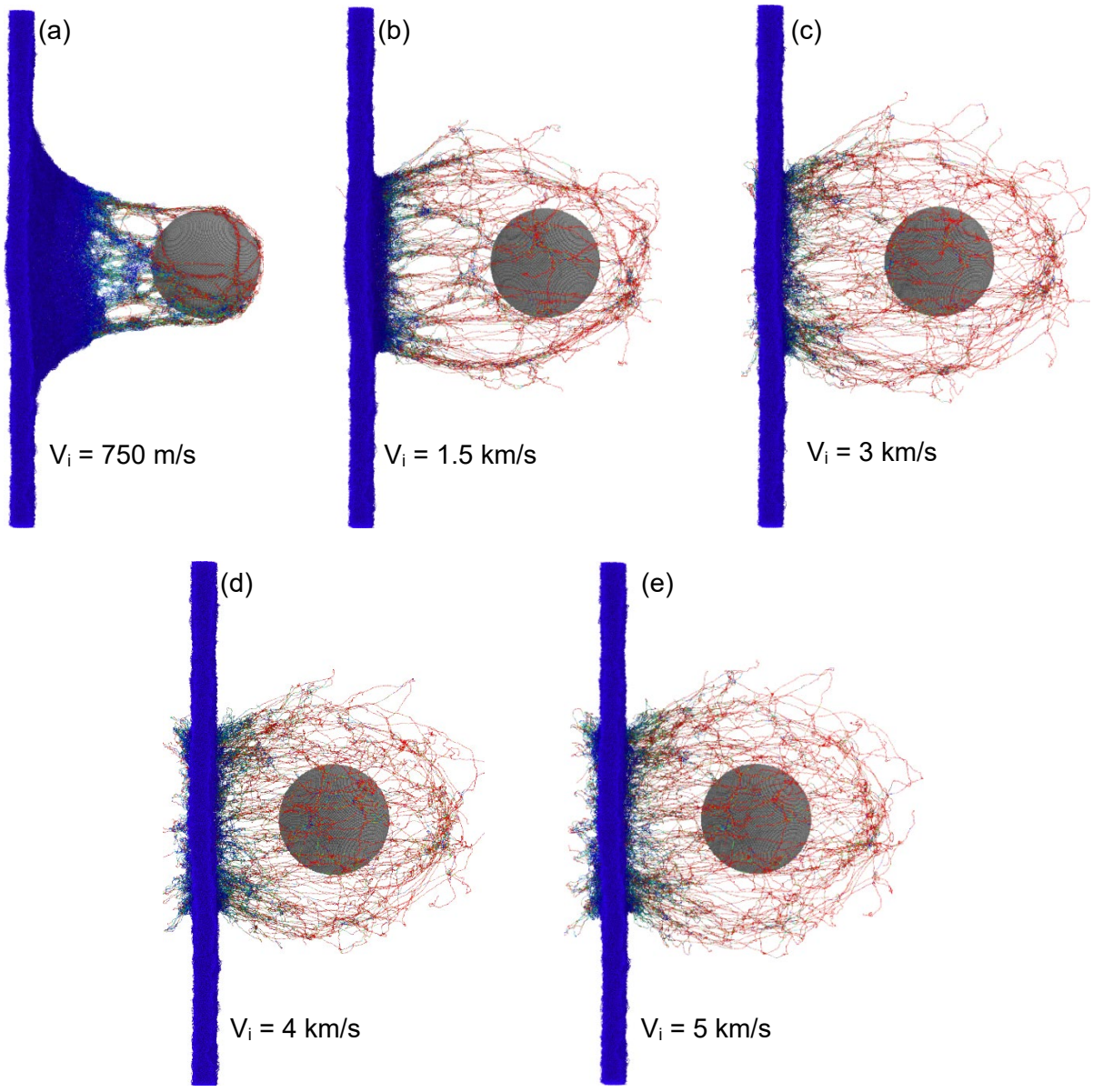

Figure S11. Snapshots of final ballistic penetration of PE for impact velocities of (a) 750 m/s, (b) 1.5 km/s, (c) 3km/s, (d) 4 km/s, and (e) 5 km/s. Failure transition from void formation and chain pull out at low-impact velocities to fragmentation and disentanglement at high impact velocities.

References

(1) Haley, B. Polymer Modeler. **2010**. https://doi.org/10.4231/D3M03Z05V.

(2) Plimpton, S. Fast Parallel Algorithms for Short–Range Molecular Dynamics. *J. Comput. Phys.* **1995**, *117*, 1–19.

(3) Mayo, S. L.; Olafson, B. D.; Goddard, W. A. DREIDING: A Generic Force Field for Molecular Simulations. *J. Phys. Chem.* **1990**, *94* (26), 8897–8909. https://doi.org/10.1021/j100389a010.

(4) Bowman, A. L.; Mun, S.; Nouranian, S.; Huddleston, B. D.; Gwaltney, S. R.; Baskes, M. I.; Horstemeyer, M. F. Free Volume and Internal Structural Evolution during Creep in Model Amorphous Polyethylene by Molecular Dynamics Simulations. *Polymer* **2019**, *170*, 85–100. https://doi.org/10.1016/j.polymer.2019.02.060.

(5) Brenner, D. W.; Shenderova, O. A.; Harrison, J. A.; Stuart, S. J.; Ni, B.; Sinnott, S. B. A Second-Generation Reactive Empirical Bond Order (REBO) Potential Energy Expression for Hydrocarbons. *J. Phys. Condens. Matter* **2002**, *14* (4), 783–802. https://doi.org/10.1088/0953-8984/14/4/312.

(6) Mun, S.; Bowman, A. L.; Nouranian, S.; Gwaltney, S. R.; Baskes, M. I.; Horstemeyer, M. F. Interatomic Potential for Hydrocarbons on the Basis of the Modified Embedded-Atom Method with Bond Order (MEAM-BO). *J Phys Chem A* **2017**, 23.

(7) Meng, Z.; Keten, S. Unraveling the Effect of Material Properties and Geometrical Factors on Ballistic Penetration Energy of Nanoscale Thin Films. *J. Appl. Mech.* **2018**, *85* (12), 121004. https://doi.org/10.1115/1.4041041.

(8) Stukowski, A. Visualization and Analysis of Atomistic Simulation Data with OVITO–the Open Visualization Tool. *Model. Simul. Mater. Sci. Eng.* **2009**, *18* (1), 015012. https://doi.org/10.1088/0965-0393/18/1/015012.

(9) Wallace, W. E.; Fischer, D. A.; Efimenko, K.; Wu, W.-L.; Genzer, J. Polymer Chain Relaxation: Surface Outpaces Bulk. *Macromolecules* **2001**, *34* (15), 5081–5082. https://doi.org/10.1021/ma002075t.

(10) Chan, E. P.; Xie, W.; Orski, S. V.; Lee, J.-H.; Soles, C. L. Entanglement Density-Dependent Energy Absorption of Polycarbonate Films via Supersonic Fracture. *ACS Macro Lett.* **2019**, *8* (7), 806–811. https://doi.org/10.1021/acsmacrolett.9b00264.

(11) Xie, W.; Lee, J.-H. Dynamics of Entangled Networks in Ultrafast Perforation of Polystyrene Nanomembranes. *Macromolecules* **2020**, *53* (5), 1701–1705. https://doi.org/10.1021/acs.macromol.9b02265.

(12) Bersted, B. H. Entanglement Network Model Relating Tensile Impact Strength and the Ductile-brittle Transition to Molecular Structure in Amorphous Polymers - Bersted - 1979 - Journal of Applied Polymer Science - Wiley Online Library. **1979**, *24* (1), 37–50. https://doi.org/1979.070240105.

(13) Hoy, R. S.; Foteinopoulou, K.; Kröger, M. Topological Analysis of Polymeric Melts: Chain Length Effects and Fast-Converging Estimators for Entanglement Length. *Phys. Rev. E* **2009**, *80* (3), 031803. https://doi.org/10.1103/PhysRevE.80.031803.

(14) Kröger, M. Shortest Multiple Disconnected Path for the Analysis of Entanglements in Two- and Three-Dimensional Polymeric Systems. *Comput. Phys. Commun.* **2005**, *168* (3), 209–232. https://doi.org/10.1016/j.cpc.2005.01.020.

(15) Shanbhag, S.; Kröger, M. Primitive Path Networks Generated by Annealing and Geometrical Methods: Insights into Differences. *Macromolecules* **2007**, *40* (8), 2897–2903. https://doi.org/10.1021/ma062457k.

(16) Tzoumanekas, C.; Theodorou, D. N. Topological Analysis of Linear Polymer Melts: A Statistical Approach. *Macromolecules* **2006**, *39* (13), 4592–4604. https://doi.org/10.1021/ma0607057.

(17) van Duin, A. C. T.; Dasgupta, S.; Lorant, F.; Goddard, W. A. ReaxFF: A Reactive Force Field for Hydrocarbons. *J. Phys. Chem. A* **2001**, *105* (41), 9396–9409. https://doi.org/10.1021/jp004368u.

(18) Dewapriya, M. A. N.; Meguid, S. A. Comprehensive Molecular Dynamics Studies of the Ballistic Resistance of Multilayer Graphene-Polymer Composite. *Comput. Mater. Sci.* **2019**, *170*, 109171. https://doi.org/10.1016/j.commatsci.2019.109171.
(19) Du, K.; Tang, Y.; Zhang, J.; Sun, T. Molecular Dynamics Modelling and Simulation of Mechanical Nanoscratching of Polystyrene. *Int. J. Nanomanufacturing* **2013**, *9* (1), 98. https://doi.org/10.1504/IJNM.2013.052888.
(20) Nouranian, S.; Tschopp, M. A.; Gwaltney, S. R.; Baskes, M. I.; Horstemeyer, M. F. An Interatomic Potential for Saturated Hydrocarbons Based on the Modified Embedded-Atom Method. *Phys. Chem. Chem. Phys. PCCP* **2014**, *16* (13), 6233–6249. https://doi.org/10.1039/c4cp00027g.
(21) Hu, S.; Sun, W.; Fu, J.; Zhang, L.; Fan, Q.; Zhang, Z.; Wu, W.; Tang, Y. Reactive Molecular Dynamics Simulations on the Thermal Decomposition of Poly Alpha-Methyl Styrene. *J. Mol. Model.* **2017**, *23* (6), 179. https://doi.org/10.1007/s00894-017-3342-8.
(22) Pionteck, J. Determination of Pressure Dependence of Polymer Phase Transitions by PVT Analysis. *Polymers* **2018**, *10* (6). https://doi.org/10.3390/polym10060578.
(23) Cha, J.-H.; Kim, Y.; Sathish Kumar, S. K.; Choi, C.; Kim, C.-G. Ultra-High-Molecular-Weight Polyethylene as a Hypervelocity Impact Shielding Material for Space Structures. *Acta Astronaut.* **2020**, *168*, 182–190. https://doi.org/10.1016/j.actaastro.2019.12.008.